# Dispersion Curve of the Helically Corrugated Waveguide Based on Helicoidal Coordinate Transform

Liang Zhang, *Senior Member,* Jack Easton, Craig R. Donaldson, Senior *Member,* Colin G. Whyte, and Adrian W. Cross

***Abstract*—This paper presents the dispersion curve study of the helically corrugated waveguide using the 2D Finite Element Method (FEM) method based on the helicoidal coordinate transform. Calculation of the dispersion curve is 60 times faster compared with 3D FEM simulation while maintaining similar accuracy. The 2D method was used to investigate the relative error between it and a 1D analytical method based on perturbation theory. Over a narrow parametric range, the 1D method has a similar dispersion (within a relative error of 3%) in comparison to the 2D/3D methods but the error greatly increased when the parameter space was expanded. Correction factors were determined to greatly enhance the 1D method accuracy over the wider parametric range. Assisted by the improved 1D method, it allows identifying the desired operating mode automatically within the multiple eigenvalues from the 2D simulation results. Therefore it can be integrated into an optimization routine to explore the applications of the helically corrugated waveguides at wider parameter ranges.**

***Index Terms*— helically corrugated waveguide, gyrotron travelling-wave amplifier, dispersion curve, helicoidal coordinate transform, Finite Element Method.**

## I. Introduction

Helically corrugated waveguide (HCW) that contains both axial and azimuthal periodicities attracts significant interest in applications such as gyro-devices [1-4], microwave undulators [5], microwave pulse compressors [6, 7], and arbitrary mode converters [8], due to its unique dispersion characteristics. By varying the geometric parameters, different dispersion curves can be generated to satisfy the requirements of different applications. For example, a dispersion curve with a constant group velocity at small axial wavenumbers over a large frequency band is desired for broadband amplification in gyrotron traveling wave amplifiers (gyro-TWAs) [9-11]. While in microwave pulse compressors, dispersion curves with large differences in the group velocities and low Ohmic loss at a wide frequency band are preferred to achieve a high compression ratio [12, 13].

The inner surface of an HCW in cylindrical coordinates can be described by $r(\theta, z) = R_0 + R_1 \cos(m_B\theta + 2\pi z/d)$, where $R_0$ and $R_1$ are the mean radius and corrugation depth, respectively. $m_B$ and $d$ are the azimuthal and axial periods. Different methods have been developed to calculate the dispersion curve of the HCW, including the 1D analytical method based on the perturbation theory [14-16], 2D eigenmode solver based on helicoidal (twist) coordinate transform [17], and 3D simulation using Finite-difference time-domain (FDTD) method or Finite Element Method (FEM) [18]. The 1D analytical equations are derived based on the assumption of small corrugation depth. It is the fastest of the three methods used however its accuracy drops as the corrugation depth increases. The 2D and 3D numerical methods suit arbitrary geometries. The 3D simulations are the simplest to set up, as various commercial software such as CST Microwave Studio, MAGIC and Ansys HFSS, can be used directly. However, large computing resources and long computing time are required to achieve high accuracy. The helicoidal coordinate transform can convert the 3D twisted HCW geometry into a straight uniform waveguide. Therefore Maxwell's equations can be solved on the 2D cross-section. The 2D method is a good balance of simulation time and accuracy. The additional drawback of the 2D and 3D numerical methods is it is difficult to identify the desired eigenmode automatically from the eigenvalues and eigenvectors solved due to the complexity of the eigenvectors, especially when the HCW operates at higher-order modes where the eigenmodes are dense in the frequency range of interest.

This paper implements and benchmarks the 2D FEM method based on the helicoidal coordinate transform. It was then used to study the 1D method and determine the correction factors to improve the accuracy. The combination of the 2D and improved 1D methods allows the automatic optimization of the HCW structures for different applications.

## II. Helicoidal coordinate transform

The 2D method was implemented and benchmarked.

This work was supported by the U.K. Engineering and Physical Sciences Research Council (EPSRC) under Grant EP/S00968X/1. Jack Easton would like to thank EPSRC for providing the PhD studentship, under reference 2434709. L. Zhang (liang.zhang @strath.ac.uk), J. Easton, C. R. Donaldson, Colin Whyte and A. W. Cross are with Department of Physics, SUPA, University of Strathclyde, Glasgow, G4 0NG, Scotland, UK.

Introducing the helicoidal coordinate transform in equ. (1), the HCW will become a straight waveguide, as illustrated in Fig. 1. The wave propagation inside the straight waveguide can therefore be solved with Neumann (for TE modes) and Dirichlet (for TM modes) boundary conditions on the 2D cross-section in the helicoidal coordinate [19].

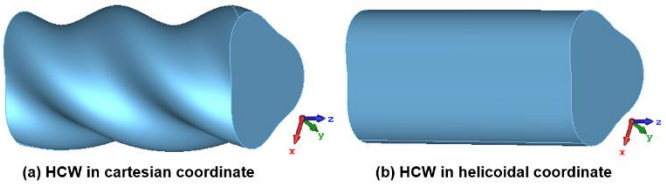


Fig. 1. HCW in Cartesian coordinate (a) and in the helicoidal coordinate (b).

$$\begin{cases} x = x'\cos(\alpha z') + y'\sin(\alpha z') \\ y = -x'\sin(\alpha z') + y'\cos(\alpha z') \\ z = z' \end{cases} \quad (1)$$

In equ. (1), $\alpha$ represents the torsion of the HCW and it is defined as

$$\alpha = -2\pi/(m_B d) \quad (2)$$

The geometric transformation matrix and the material property transformation matrix between the helicoidal coordinate and the Cartesian coordinate are expressed in equ. (3) and (4).

$$J(x',y',z') = \begin{bmatrix} \cos(\alpha z') & \sin(\alpha z') & \alpha y'\cos(\alpha z') - \alpha x'\sin(\alpha z') \\ -\sin(\alpha z') & \cos(\alpha z') & -\alpha x'\cos(\alpha z') - \alpha y'\sin(\alpha z') \\ 0 & 0 & 1 \end{bmatrix} \quad (3)$$

$$T(x',y') = \begin{bmatrix} 1 & 0 & \alpha y' \\ 0 & 1 & -\alpha x' \\ \alpha y' & -\alpha x' & 1+\alpha^2(x'^2+y'^2) \end{bmatrix} \quad (4)$$

The Maxwell's equations can be solved either with the FDTD method [20, 21] or the FEM method [22]. FDTD is easier to implement, however sufficiently small mesh grid will be needed to accurately preserve the curved face to achieve high accuracy of the eigenfrequencies. In this paper, the FEM method was used. The weak formulation of Maxwell's equations in the helicoidal coordinate $(x', y', z')$ can be written as [22]

$$\begin{aligned} R(k_z, \boldsymbol{E}, \boldsymbol{E}') = \int_\Omega & \mu_r^{-1}\left(\nabla_t \times \boldsymbol{E_t} + (\nabla_t E_z - ik_z \boldsymbol{E_t}) \times \boldsymbol{e}^{z'}\right) \\ & \times \overline{(\nabla_t \times \boldsymbol{E_t'} + (\nabla_t E_z' - \imath k_z \boldsymbol{E_t'}) \times \boldsymbol{e}^{z'}}\, dx'dy' \\ & -k_0^2 \int_\Omega \varepsilon_r\left(\boldsymbol{E_t} + E_z\boldsymbol{e}^{z'}\right) \cdot \overline{\boldsymbol{E_t'} + E_z'\boldsymbol{e}^{z'}}\, dx'dy' = 0 \end{aligned} \quad (5)$$

where $\varepsilon_r, \mu_r$ are the dielectric constant and permeability of the waveguide media respectively. Equ. (5) can be expanded and re-organized as equ. (6). It shows the relationship between the axial wavenumber $k_z$ and the free-space wavenumber $k_0$, which is also the dispersion curve.

$$\begin{aligned} & \int_\Omega \left( (\mu_r^{-1}\nabla_t \times \boldsymbol{E_t}) \cdot (\nabla_t \times \overline{\boldsymbol{E_t'}}) \right. \\ & + (\mu_r^{-1}\nabla_t \times \boldsymbol{E_t}) \cdot (\nabla_t \overline{E_z'} \times \boldsymbol{e}^{z'}) \\ & + (\mu_r^{-1}(\nabla_t E_z \times \boldsymbol{e}^{z'})) \cdot (\nabla_t \times \overline{\boldsymbol{E_t'}}) \\ & + (\mu_r^{-1}(\nabla_t E_z \times \boldsymbol{e}^{z'})) \cdot (\nabla_t \overline{E_z'} \times \boldsymbol{e}^{z'}) \\ & + ik_z(\mu_r^{-1}\nabla_t \times \boldsymbol{E_t}) \cdot (\overline{\boldsymbol{E_t'}} \times \boldsymbol{e}^{z'}) \\ & + ik_z(\mu_r^{-1}(\nabla_t E_z \times \boldsymbol{e}^{z'})) \cdot (\overline{\boldsymbol{E_t'}} \times \boldsymbol{e}^{z'}) \\ & - ik_z\left(\mu_r^{-1}(\boldsymbol{E_t} \times \boldsymbol{e}^{z'})\right) \cdot (\nabla_t \times \overline{\boldsymbol{E_t'}}) \\ & - ik_z\left(\mu_r^{-1}(\boldsymbol{E_t} \times \boldsymbol{e}^{z'})\right) \cdot (\nabla_t \overline{E_z'} \times \boldsymbol{e}^{z'}) \\ & + k_z^2\left(\mu_r^{-1}(\boldsymbol{E_t} \times \boldsymbol{e}^{z'})\right) \cdot (\overline{\boldsymbol{E_t'}} \times \boldsymbol{e}^{z'}))dx'dy' \\ & - k_0^2 \int_\Omega ((\varepsilon_r \boldsymbol{E_t}) \cdot \overline{\boldsymbol{E_t'}} + (\varepsilon_r E_z \boldsymbol{e}^{z'}) \cdot \overline{\boldsymbol{E_t'}} + (\varepsilon_r \boldsymbol{E_t}) \cdot (\overline{E_z'}\boldsymbol{e}^{z'}) + \\ & (\varepsilon_r E_z \boldsymbol{e}^{z'}) \cdot (\overline{E_z'}\boldsymbol{e}^{z'}))dx'dy' = 0 \end{aligned} \quad (6)$$

Using the Galerkin method and introducing the finite element approximation [23], the weak formulation will become a generalized eigenvalue problem as the function of $k_z$ and $k_0$, and $E_z'$, $\boldsymbol{E_t'}$ are the weights on the discrete meshes. The problem will become a matrix system, and the eigen equation (6) becomes

$$M_1\boldsymbol{u} + ik_z M_2\boldsymbol{u} + k_z^2 M_3\boldsymbol{u} - k_0^2 M_4\boldsymbol{u} = 0 \quad (7)$$

where $M_1$, $M_2$, $M_3$ and $M_4$ are the matrics associated with the meshes, and $\boldsymbol{u}$ is the eigenvectors. The eigenvalue problem can either solve $k_0$ by fixing $k_z$, or $k_z$ by fixing $k_0$. The former one is simpler and is easier to post-process as $k_0$, which can be converted into frequency using $k_0 c/2\pi$, but it needs to be positive real values for a practical system. The latter one is more complicated and takes longer computing time however it provides additional information on the eigenmodes. The imaginary part of $k_z$ is the attenuation factor of the eigenmode. The eigenfrequencies present in this paper were all solved by fixing the $k_z$ values.

Equ. (4) shows that in the helicoidal coordinate, the material properties of waveguide media inside the HCW are no longer homogeneous. The mesh has a large impact on the quality of the FEM results, especially when calculating the eigenvalues. Therefore, special care was taken when determining the mesh as phase errors can be introduced if the mesh uniformity, which was defined by the maximum size to the minimum size, is poor. A uniform mesh will help to achieve more accurate results and reduce the number of iterations required to reach convergence. Different mesh generators were tested, and the mesh qualities were evaluated. DistMesh which has the best mesh uniformity was chosen to generate the mesh for the HCW [24]. An example of the mesh generated by DistMesh is shown in Fig. 2. The uniformity of the meshes is 0.85, which is better than ~0.7 from the standard mesh generator. The eigenmode equation was then solved by the open-sourced FEM solver GetDP [25], which allows defining the input data with a closed form of the symbolic mathematical expressions based on the weak formulation.

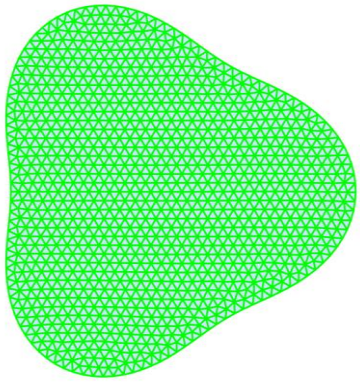

Fig. 2. Example of the mesh generated by DistMesh.

After the calculation, the eigenvalues and eigenvectors at individual $k_z$ were collected and post-processed to get the eigenfrequencies of the supported modes in the HCW as well as their eigenvectors in the Cartesian coordinate.

The proposed FEM method to calculate the dispersion curve is ideal for the infinite length of the HCW or other twisted waveguide structure. The torsion $\alpha$, which associates with the periodicity of the HCW and is defined in equ. (2), implies that the periodic condition has been used in the coordinate conversion. For the finite length, from our experience of designing the mode converters using the HCW [13], the dispersion curve will be slightly distorted if the period number is too small due to a weak mode coupling strength. However, at more than 6 periods of HCW the dispersion will remain constant satisfying most applications.

## III. Convergence Study and Benchmark of the Simulation Results

Fig. 3 shows the convergence study of the 2D FEM calculation at different mesh sizes. In the calculation, the dimensions were chosen as $R_0$=1.45 mm, $R_1$=0.23 mm, $m_B$=3, and $d$=3.20 mm, which has been used as the interaction circuit of a W-band gyro-TWA [2]. The average size of the mesh cell was defined by $R_0/N$, and the computing time was the overall CPU time for calculating 101 eigen points that cover the dispersion curve. As $N$ increases, the differences in the calculated eigenvalues at different $N$ values will become smaller. To show the convergence of the calculation, the results at $N = 80$ were defined as reference values, and the relative error $\delta$ at different $N$ values was defined as

$$\delta(k_z) = f_N(k_z)/f_{N=80}(k_z) - 1 \qquad (8)$$

The maximum relative error was defined as $\delta_{max} = \max(|\delta(k_z)|)$, and the standard relative error was defined as $\delta_{std} = \mathrm{std}(\delta(k_z))$. Fig. 3 shows that less than 0.05% difference in the calculated eigenvalues at different mesh cell sizes can be achieved with $N > 40$ and the computing time was less than 60 seconds.

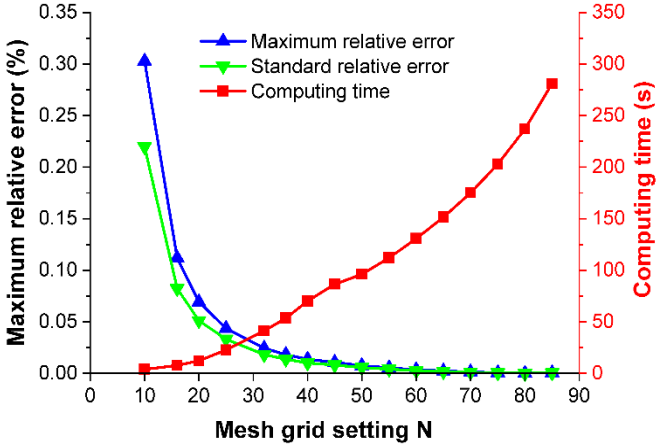


Fig. 3. The relative errors and the computing times (101 data points) of the 2D FEM simulation at different mesh cell numbers.

The interested eigenmode was coupled by the $TE_{11}$ mode in the circular waveguide and the first spatial harmonic of the $TE_{21}$ mode. A comparison of the 1D analytical method to the 2D FEM and the 3D FEM simulation using the commercial EM package CST Microwave Studio, as well as the measurement results [2] is shown in Fig. 4. In this case the relative error $\eta$ is defined by

$$\eta(k_z) = f_{1D/3D/meas.}(k_z)/f_{2D}(k_z) - 1 \qquad (9)$$

where $f_{1D/3D/meas.}$ is the eigenfrequency of the 1D method, 3D method or the experimental measurement, and $f_{2D}$ is the result from the 2D FEM method at $N = 80$. The difference between the 2D and 3D simulations are well below 0.05%, and both results have relative errors of less than 0.5% compared with the measurement, indicating both methods have excellent accuracy. Since the HCW is a periodic structure, a periodic boundary condition can be applied in the eigenmode solver in CST based on the Floquet theory. Only one single period of the HCW is modeled and calculated in the 3D simulation to save computing time. However, the 3D simulations still took about 10 hours to calculate 101 points in the dispersion curve with a mesh number of $3.5\times10^5$. The 2D method was about 60 times faster than the 3D simulation. The speedup would be more significant when the HCW operates at the higher-order modes, where the mesh number would increase more rapidly in a 3D volume than on the 2D cross-section.

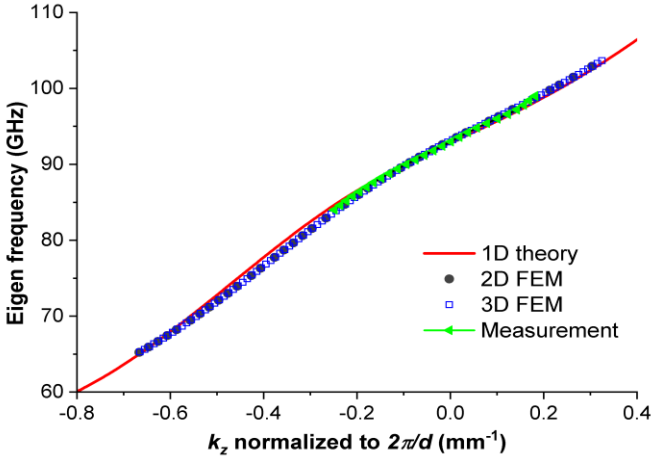


(a)

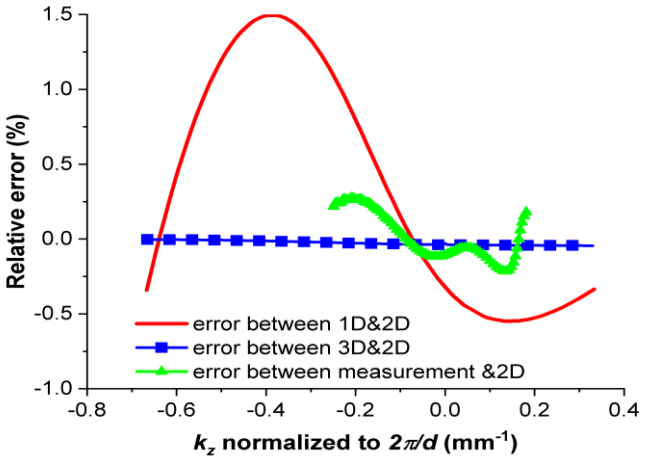


(b)

Fig. 4. Dispersion curves of the 1D, 2D, 3D simulation results and the experimental measurement (a), and the relative errors compared with the 2D simulation results (b).

The 1D analytical method had played an important role in the

preliminary design of the HCW since it is significantly faster than the other methods. The maximum relative error of the 1D theory for the calculated dimension set was about 1.5% over the interested frequency range for this group of geometries, which is not high enough for the precise design. For example, the magnetic field strength $B$ for the beam-wave interaction follows the synchronize condition $\omega(k_z = 0) \approx s\eta B/\gamma$, where $\eta$ is the electron charge-to-mass ratio, $s$ is the harmonic number, and $\gamma$ is the Lorentz factor. The detuning of $B$ was less than 1.0% in the particle-in-cell simulations, which was verified by experimental measurement. Therefore a similar level of accuracy is required for the prediction of the dispersion curve to save the computing time in the heavy particle-in-cell simulations. In the microwave pulse compressor, the input frequency sweep signal is entirely determined by the dispersion relation of the HCW. A small error in the dispersion may cause a large error in the group velocity $v_g = d\omega/dk_z$ at $k_z \approx 0$, and result in a significant reduction in the compression ratio.

The 2D FEM method allows examination of the accuracy of the 1D method in a wider geometric parameter range. Fig. 5 shows the relative errors of the 1D and 2D methods at different corrugation depths and periods. The results have been normalized to the mean waveguide radius to form a universal conclusion. The relative errors were calculated by the average of the square sum of equ. (9) over $-0.5 \leq k_z d/2\pi \leq 0.5$. The 1D analytical method has a relative error of less than 3% at a relatively small geometric parameter range, where $R_1/R_0$<15.0% and $2.0 \leq d/R_0 \leq 4.2$. The errors can be as large as 30% at small or large periods and deep corrugation depth. When the corrugation period is small, the mode coupling is strong and the transient of the mode patterns, for example from the $TE_{11}$ mode into the $TE_{21}$ mode, is rapid and does not satisfy the smooth conversion of the field pattern required in the perturbation theory. While at larger corrugation periods, the coupling point locates at large $k_z$, the coupling strength is weak and its bandwidth is narrow. The error at large corrugation depth mainly occured due to improper calculation of the cutoff frequency using the mean radius $R_0$, as the cross-section of the HCW has been deformed significantly.

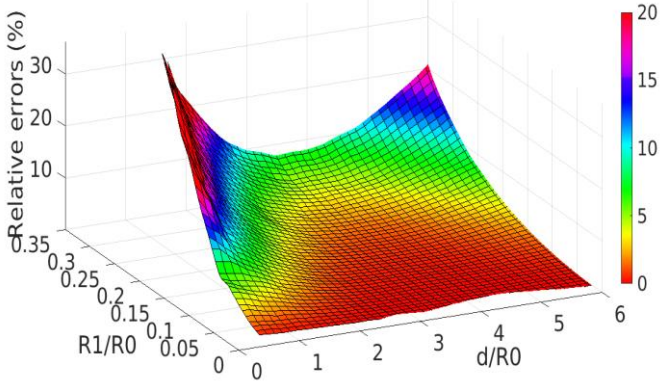


Fig. 5. The relative error of 2D FEM and the 1D theoretical model as functions of the corrugation depth and period.

## IV. Correction Factors to 1D Analytical Method

The 2D FEM method is optimal as it balances accuracy with computing time. However, the biggest challenge is to identify the dispersion curve of the desired operating mode automatically from the calculated results, which makes it difficult to be integrated into an optimization routine to explore large parameter space. The 1D results can be a great reference point to identify the desired eigenvalues and electric and magnetic field patterns in the 2D simulations if their accuracy can be higher over a broader parameter range. This was achieved by applying corrections on $R_0, R_1$in the perturbation theory for different $R_1$ and $d$ values.

For each geometry set $R_0, R_1$ and $d$, the dispersion curve from 2D simulations was manually picked and set as the 'true' value. Then the optimal correction factors for $R_0, R_1$ in the 1D method were chosen using the genetic optimization algorithm where the optimization target was the minimum difference between the 1D and 2D results. The correct factors were normalized to $R_0$ therefore it suits the HCWs operating at different frequencies. A plot of the correction factors is shown in Fig. 6. When the corrugation depth becomes larger, a smaller factor less than 1.0 should apply to the mean radius, indicating the cutoff frequency of the modes become larger.

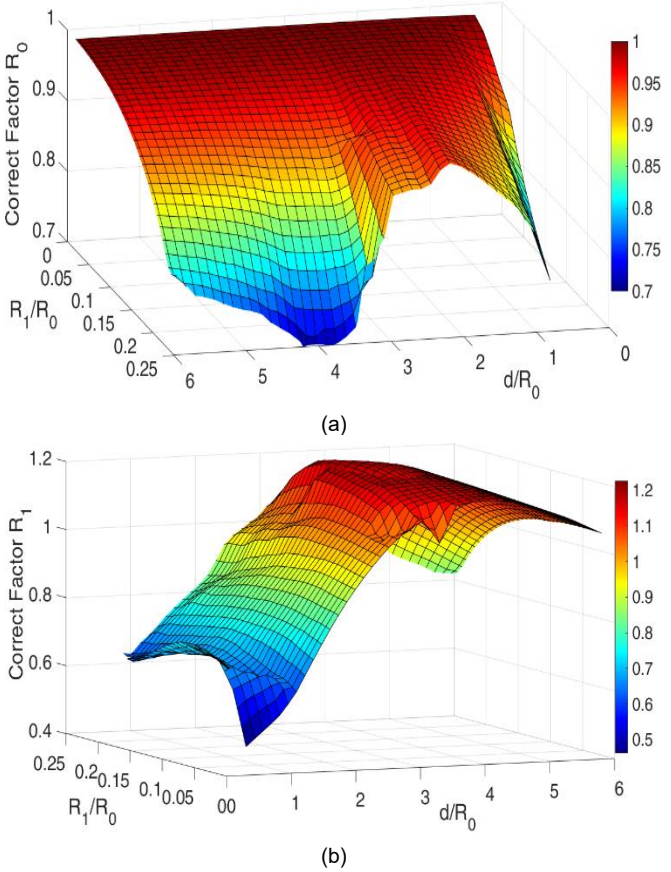


Fig. 6. The correction factors of $R_0$ (a) and $R_1$ (b) at different corrugation depths and periods.

With the correction factors, the differences between the 1D method and the 2D method become much smaller, as shown in Fig. 7. It is less than 1% in the major parameter range, and the maximum difference is less than 3%. Expression of the correction factors will be more convenient and easier to use. However, it is challenging to find empirical formulas in simple forms to fit the correction factors over the whole parameter range. At a smaller parameter range of $0 \leq R_1/R_0 \leq 0.22$ and

$1 \le d/R_0 \le 4$, empirical formulas in simple forms were found in equ. (10). The maximum relative error was smaller than 2% and around 1% at the major parameter range, as shown in Fig. 8.

$$\alpha = 1.03 - 0.03 * 2^{22.3x^2+6.0x|y-2.24|-0.17(y-2.24)^2}$$
$$\beta = 0.51 + 0.72 * 1.50^{-40.0(x-0.13)^2+0.52|(x-0.13)(y-3.71)|-0.53(y-3.71)^2} \quad (10)$$

where $x = R_1/R_0$, and $y = d/R_0$, $\alpha$ and $\beta$ are the correction factors to $R_0$ and $R_1$, respectively.

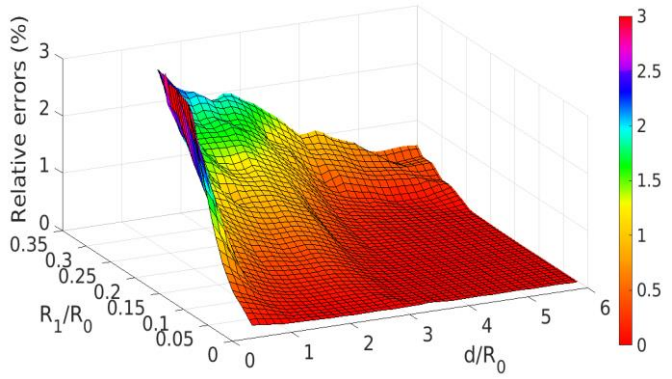


Fig. 7. The relative error of 2D FEM and the 1D theoretical model as the functions of corrugation depth and period with the correction factor in Fig. 6.

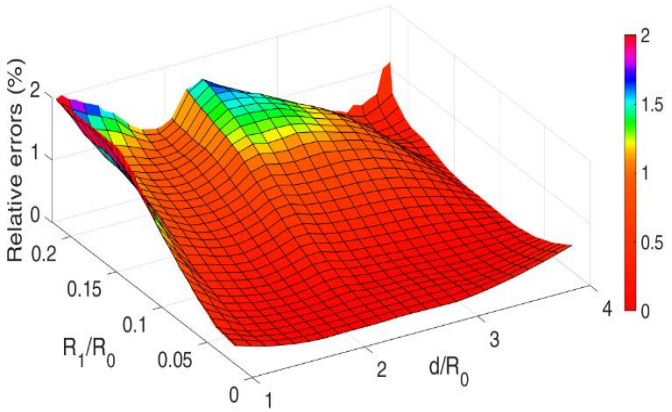


Fig. 8. The relative error of 2D FEM and the 1D theoretical model as the functions of corrugation depth and period with the correction factor in equ. (10).

## V. Discussion and Conclusion

In this paper, the 2D FEM method based on the helicoidal coordinate transform was implemented and benchmarked to calculate the dispersion curve of the helically corrugated waveguide. It provides a great balance between computing accuracy and speed. The 2D FEM method is more than 60 times faster than the 3D FEM simulations.

The 1D analytical method based on perturbation theory is the fastest however the accuracy drops for shorter periods and deeper corrugation depths. The accuracy of the 1D method was investigated, and the empirical formulas of the correct factors for the geometric parameters were found to fit best when based on the 2D simulation results. The relative errors were less than 2% in the parameter ranges of $0 \le R_1/R_0 \le 0.22$ and $1 \le d/R_0 \le 4$. This covers the parameter range of the major applications of the helically corrugated waveguide.

More accurate 1D results make this method ideal for reference points that can be used for the identification of the operating mode in the 2D method, especially if in the difficult scenario of the HCW operating at higher-order mode. This allows the integration of the 2D method into an optimization routine to explore the applications of the HCW over wide parameter ranges.

## A cknowledgment

Data underpinning this publication are openly available from the University of Strathclyde at: https://doi.org/10.15129/fe4f7b47-de42-45bc-81c3-575749d44dc2

## References

[1] W. He, C. R. Donaldson, L. Zhang, K. Ronald, P. McElhinney, and A. W. Cross, "High Power Wideband Gyrotron Backward Wave Oscillator Operating towards the Terahertz Region," *Phys. Rev. Lett.,* vol. 110, no. 16, p. 165101, 2013, doi: 10.1103/PhysRevLett.110.165101.

[2] W. He, C. R. Donaldson, L. Zhang, K. Ronald, A. D. R. Phelps, and A. W. Cross, "Broadband Amplification of Low-Terahertz Signals Using Axis-Encircling Electrons in a Helically Corrugated Interaction Region," *Phys. Rev. Lett.,* vol. 119, no. 18, p. 184801, Oct. 2017, doi: 10.1103/PhysRevLett.119.184801.

[3] S. V. Samsonov *et al.*, "CW Ka-Band Kilowatt-Level Helical-Waveguide Gyro-TWT," *IEEE Trans. Electron Devices,* vol. 59, no. 8, pp. 2250-2255, 2012, doi: 10.1109/TED.2012.2196703.

[4] S. V. Mishakin, S. V. Samsonov, and G. G. Denisov, "A Helical-Waveguide Gyro-TWT at the Third Cyclotron Harmonic," *IEEE Trans. Electron Devices,* vol. 62, no. 10, pp. 3387-3392, 2015, doi: 10.1109/TED.2015.2460265.

[5] L. Zhang, W. He, J. Clarke, K. Ronald, A. D. R. Phelps, and A. W. Cross, "Microwave Undulator Using a Helically Corrugated Waveguide," *IEEE Trans. Electron Devices,* vol. 65, no. 12, pp. 5499-5504, 2018, doi: 10.1109/TED.2018.2873726.

[6] L. Zhang *et al.*, "Experimental Study of Microwave Pulse Compression Using a Five-Fold Helically Corrugated Waveguide," *IEEE Trans. Microwave Theory Techn.,* vol. 63, no. 3, pp. 1090-1096, 2015, doi: 10.1109/TMTT.2015.2393882.

[7] S. V. Samsonov *et al.*, "Compression of Frequency-Modulated Pulses using Helically Corrugated Waveguides and Its Potential for Generating Multigigawatt rf Radiation," *Phys. Rev. Lett.,* vol. 92, no. 11, p. 118301, Mar. 2004, doi: 10.1103/PhysRevLett.92.118301.

[8] D. B. McDermott, J. Pretterebner, C. K. Chong, C. F. Kinney, M. M. Razeghi, and N. C. Luhmann, "Broadband linearly polarized beat-wave TEm1 TE11 mode converters," *IEEE Trans. Microwave Theory Techn.,* vol. 44, no. 2, pp. 311-317, 1996, doi: 10.1109/22.481581.

[9] G. G. Denisov *et al.*, "Gyrotron Traveling Wave Amplifier with a Helical Interaction Waveguide," *Phys. Rev. Lett.,* vol. 81, no. 25, pp. 5680-5683, Dec. 1998, doi: 10.1103/PhysRevLett.81.5680.

[10] V. L. Bratman *et al.*, "High-Gain Wide-Band Gyrotron Traveling Wave Amplifier with a Helically Corrugated Waveguide," *Phys. Rev. Lett.,* vol. 84, no. 12, pp. 2746-2749, 2000, doi: 10.1103/PhysRevLett.84.2746.

[11] C. R. Donaldson *et al.*, "8-Fold Helically Corrugated Interaction Region for High Power Gyroresonant THz Sources," *IEEE Electron Device Letters,* vol. 42, no. 10, pp. 1544-1547, 2021, doi: 10.1109/LED.2021.3105435.

[12] V. L. Bratman *et al.*, "Generation of 3 GW microwave pulses in X-band from a combination of a relativistic backward-wave oscillator and a helical-waveguide compressor," *Physics of Plasmas,* vol. 17, no. 11, Nov 2010, Art no. 110703, doi: 10.1063/1.3505825.

[13] C. R. Donaldson *et al.*, "Fivefold Helically Corrugated Waveguide for High-Power W-Band Gyro-Devices and Pulse Compression,"

*IEEE Trans. Electron Devices,* vol. 69, no. 1, pp. 347-352, 2022, doi: 10.1109/TED.2021.3130846.

[14] G. G. Denisov and M. G. Reznikov, "Corrugated cylindrical resonators for short-wavelength relativistic microwave oscillators," *Radiophysics and Quantum Electronics,* vol. 25, no. 5, pp. 407-413, May 1982, doi: 10.1007/bf01035315.

[15] L. Zhang *et al.*, "Multi-Mode Coupling Wave Theory for Helically Corrugated Waveguide," *IEEE Trans. Microwave Theory Techn.,* vol. 60, no. 1, pp. 1-7, Jan. 2012, doi: 10.1109/TMTT.2011.2170848.

[16] S. J. Cooke and G. G. Denisov, "Linear theory of a wide-band gyro-TWT amplifier using spiral waveguide," *IEEE Trans. Plasma Sci.,* vol. 26, no. 3, pp. 519-530, 1998, doi: 10.1109/27.700786.

[17] S. V. Mishakin and S. V. Samsonov, "Analysis of Dispersion and Losses in Helically Corrugated Metallic Waveguides by 2-D Vector Finite-Element Method," *IEEE Trans. Microwave Theory Techn.,* vol. 59, no. 9, pp. 2189-2196, Sept. 2011, doi: 10.1109/TMTT.2011.2160201.

[18] G. Burt *et al.*, "Dispersion of helically corrugated waveguides: Analytical, numerical, and experimental study," *Physical Review E,* vol. 70, no. 4, p. 046402, Oct. 2004, doi: 10.1103/PhysRevE.70.046402.

[19] D. M. Pozar, *Microwave Engineering*. Wiley, 2011.

[20] J. L. Wilson, A. E. Fathy, Y. W. Kang, and C. Wang, "Applications of Twisted Hollow Waveguides as Accelerating Structures," *IEEE Trans. Nucl. Sci.,* vol. 56, no. 3, pp. 1479-1486, 2009, doi: 10.1109/TNS.2009.2017534.

[21] J. L. Wilson, C. Wang, A. E. Fathy, and Y. W. Kang, "Analysis of Rapidly Twisted Hollow Waveguides," *IEEE Trans. Microwave Theory Techn.,* vol. 57, no. 1, pp. 130-139, 2009, doi: 10.1109/TMTT.2008.2009042.

[22] A. Nicolet and F. Zolla, "Finite element analysis of helicoidal waveguides," (in En), *IET Science, Measurement & Technology,* vol. 1, no. 1, pp. 67-70, 2007, doi: 10.1049/IET-SMT:20060042.

[23] A. Ern and J. L. Guermond, *Theory and Practice of Finite Elements*. Springer New York, 2004.

[24] P.-O. Persson and G. Strang, "A Simple Mesh Generator in MATLAB," *SIAM Rev.,* vol. 46, no. 2, pp. 329–345, 2004, doi: 10.1137/s0036144503429121.

[25] P. Dular, C. Geuzaine, F. Henrotte, and W. Legros, "A general environment for the treatment of discrete problems and its application to the finite element method," *IEEE Trans. Magn.,* vol. 34, no. 5, pp. 3395-3398, 1998, doi: 10.1109/20.717799.